Exploration of the prerecombination universe with a high-dimensional model of an additional dark fluid

Michael Meiers[*] and Lloyd Knox[†]

*Department of Physics and Astronomy, University of California Davis,
One Shields Avenue, Davis, California 95616, USA*

Nils Schöneberg[‡]

*Institut de Ciències del Cosmos (ICCUB), Facultat de Física, Universitat de Barcelona (IEEC-UB),
Martí i Franqués, 1, E08028 Barcelona, Spain*

We implement and explore high-dimensional generalized dark matter (HDGDM) with an arbitrary equation of state as a function of redshift as an extension to Λ cold dark matter. Exposing this model to cosmic microwave background, baryon acoustic oscillations, and supernova data, we demonstrate that the use of marginalized posterior distributions can easily lead to misleading conclusions on the viability of a high-dimensional model such as this one. We discuss such pitfalls and corresponding mitigation strategies, which can be used to search for an observationally favored region of the parameter space. We further show that the HDGDM model in particular does show promise in terms of its ability to ease the Hubble tension once such techniques are employed, and we find interesting features in the best-fitting equation of state that can serve as an inspiration for future model building.

I. INTRODUCTION

Intensity and polarization maps of the cosmic microwave background (CMB) are highly sensitive to forces affecting the plasma in the two decades of scale factor evolution prior to recombination (e.g., [1,2]). As such, measurements of these maps are capable of constraining fairly high-dimensional models of an additional dark component that is dynamically important during that epoch. To explore the constraints from data on this epoch we extend the Lambda cold dark matter (ΛCDM) model to include a fluid component modeled as "generalized dark matter" (GDM) [3] with viscosity and sound-speed parameters as free (time-independent) parameters and an equation of state parameter $w_g \equiv P_g/\rho_g$ that is a (approximately) free function of redshift. We refer to this model as high-dimensional generalized dark matter, or HDGDM.

This is a purely phenomenological model intended to enable a search for a variety of potential departures from ΛCDM to see, given cosmological data, what departures are preferred, what are allowed, and what are ruled out. A discovery of a preference for a departure from ΛCDM might then serve as guidance for future, more physical, model building.

Our search procedure is a "bottom-up" approach, driven by the data, distinguished from the analyses of lower-dimensional and more theoretically motivated models in [4–13] which might instead be called "top-down." In addition to presenting our HDGDM model, we present some initial lessons about use of such high-dimensional models for exploration of the implications of data.

The HDGDM model is similar to a model used in two prior reconstructions of, in one case the expansion rate, and in another the dark energy fraction, as functions of redshift. In [14] the authors used a GDM model with its density history determined by its parametrized values at a set of control points in redshift to reconstruct $H(z)$ from the first release of cosmological data from Planck [15]. More recently, the authors of [16] used a very similar GDM model to reconstruct the fraction of energy density in dark energy from $z = 0$ to $z = 10^5$ using various combinations of cosmological datasets.

We find that exploration of high-dimensional models brings to the fore some issues of data analysis and inference that are not at present in the more commonly explored lower-dimensional models. First and foremost, there are challenges that arise from the "curse of dimensionality." Standard techniques for determining joint and marginal posterior probability distributions can end up taking a prohibitively long time to converge.

Even if one can perform Bayesian inference in a high-dimensional model space, an additional pitfall remains that

---
[*]mcmeiers@ucdavis.edu
[†]lknox@ucdavis.edu
[‡]nils.science@gmail.com

perfectly good regions of parameter space can effectively get lost, overwhelmed by much greater volume in other regions of parameter space. Such volume effects have been noted in lower-dimensional models too, and in models of early dark energy (EDE) in particular (see the recent EDE review [11] and references therein). The effective obscuration of regions that provide perfectly good fits leads us to a conclusion that if our goal is to find new and interesting ways of fitting the data, marginalization over vast regions of parameter space is probably not what we want to be doing.

We ground this discussion of the perils of exploring high-dimensional model spaces with an application of our HDGDM model inspired by the "Step" model of [10]. In this model a light relic becomes nonrelativistic and then decays into a massless particle. The equation-of-state parameter for this component thus begins as $w = 1/3$, drops a bit, and then returns to $w = 1/3$. They find some preference for such a component with the transition near $z \simeq 20\,000$. Interestingly, they find that this region of parameter space also leads to a higher H_0 and thus a reduction of the tension with the most recent measurement by the SH$_0$ES Collaboration [17].

We use the HDGDM model to further explore this hint that a nontrivial evolution near $z \sim 20\,000$ can have a strong impact on the Hubble tension. For this, we use a component that at both higher z and lower z is evolving like a light relic. Depending on how broadly we open up the prior constraints on w_g, the statistical signal supporting the interesting solution of [10] can effectively disappear.

We also find in this analysis the curious result that *adding* information (by restricting the allowed range of w_g values) leads to a *broader* marginal posterior probability distribution for H_0. We attribute this unusual behavior to volume effects arising from implicit priors. Interpretation of results thus requires grappling with this dependence on priors. We also discuss a few mitigation strategies that can allow for effective model and parameter searching even in this high-dimensional parameter space. In particular, we outline the importance of likelihood minimization and the corresponding challenges.

In Sec. II we introduce the broad details of our HDGDM model and its implementation as an extension to the publicly available Einstein-Boltzmann solver, CLASS. We also present some validation of this numerical code via comparison with existing CLASS capabilities. In Sec. III we present our exploration of the parameter space, and lessons learned. We conclude in Sec. IV.

II. HIGH-DIMENSIONAL GENERALIZED DARK MATTER

In the following subsections, we introduce HDGDM, which we use to build extensions of ΛCDM. Our extended models contain all standard ΛCDM constituents, including both dark components, and further introduce a realization of GDM [18]. We first review the critical features of a GDM

material, then present our realization of the model for numeric applications in CLASS along with our validation of the implementation.

A. A brief introduction to generalized dark matter

Our high-dimensional modeling uses GDM, conceived initially by W. Hu [18]. In this subsection, we summarize the essential details of this model. For a deeper dive into the topic and to explore related theories, see [19].

1. General tensor field description

We take the general decomposition of an energy-momentum tensor as

$$T^\mu_{\ \nu} = \rho(u^\mu u_\nu) + (u^\mu q_n u + q^\mu u_\nu) + P(u^\mu u_\nu + \delta^\mu_\nu) + \Sigma^\mu_{\ \nu},$$
(1)

where ρ, P, u^μ, q^μ and Σ^μ_ν are the energy density, pressure, four-velocity, heat flux, and anisotropic stress respectively. The latter two are orthogonal to the four-velocity and vanish in an unperturbed Friedmann–Lemaître–Robertson–Walker spacetime. The anisotropic stress is traceless and can be nonzero at perturbative levels. Our work uses the Landau-Lifshitz frame, which sets the four-velocity so that the heat flux vanishes at all perturbative levels.

The equation-of-state parameter $w \equiv P/\rho$ sets the background relationship between the pressure and the energy density. Traditional treatments restrict to a constant w, but it is a time-dependent function in general cases such as GDM. Perturbations have an adiabatic speed of sound set by

$$c_a^2 \equiv \frac{\dot{P}}{\dot{\rho}} = w - \frac{\dot{w}}{3\mathcal{H}(1+w)},$$
(2)

where the dot denotes the derivative with respect to conformal time and $\mathcal{H} \equiv \dot{a}/a$. The equality is purely a consequence of energy-momentum conservation $\nabla_\mu T^\mu_{\ \nu} = 0$, which requires that

$$\dot{\rho} = -3\mathcal{H}(1+w)\rho$$
(3)

is separately satisfied for each noninteracting component of the Universe. Note that $c_a^2 \neq w$ unless we have constant w. When subscripts are left out, we generally refer to the GDM species. However, we will include subscripts when ambiguity may arise.

2. GDM closure relations

At a perturbative level, two modifications to the standard treatment of perfect fluids close the evolution equations of GDM. The first is the inclusion of nonadiabatic pressure (NAP) contributions denoted $\Pi_{\text{nap}} = \Pi - c_a^2 \delta$ where Π is the isotropic pressure perturbation defined by the trace of

the spacelike component of the energy-momentum tensor $T^i_{\ i} = 3\bar{\rho}(w + \Pi)$ and $\delta = \delta\rho/\bar{\rho}$ with $\bar{\rho}$ the background energy density.

The equation of state parameter alone is insufficient to specify the NAP contributions, and models must specify this term as an additional input. As the NAP contributes in a gauge-invariant way, any choice must respect this property. Hu's original proposal has $\Pi_{\rm nap} \propto \delta$ in the rest frame of the material, which is lifted to a gauge-invariant statement in Fourier space as [19]

$$\Pi_{\rm nap} = (c_s^2 - c_a^2)\hat{\Delta}, \qquad (4)$$

$$\hat{\Delta} = \delta + 3(1 + w)\mathcal{H}\theta/k^2, \qquad (5)$$

where the free parameter, c_s^2, can be thought of as the rest frame speed of sound. The divergence of velocity perturbation θ is defined to satisfy $\bar{\rho}(1 + w)\theta = ik^i\delta T^0_{\ i}$. In the perturbation's rest frame $\theta = 0$, we see that $\hat{\Delta} = \delta$. Thus, the general expression $\Pi = c_a^2\delta + \Pi_{\rm nap} = c_a^2\delta + (c_s^2 - c_a^2)\hat{\Delta}$ reduces to $\Pi = c_s^2\delta_{\rm rest}$ which supports the identification of c_s^2 as an effective speed of sound in the rest frame.

The second modeling choice supports growing modes for anisotropic stress. Here we differ slightly from Hu's original suggestion and use a change proposed by [19]. In [20] the fourier space scalar anisotropic stress perturbation, σ, is defined by

$$\sigma = -\frac{1}{\bar{\rho}(1 + w)}\left(\hat{k}_i\hat{k}_j - \frac{1}{3}\delta_{ij}\right)\Sigma^{ij}. \qquad (6)$$

This quantity is also gauge invariant, but neither Einstein's nor conservation equations specify its evolution.

Hu originally motivated the closure relation choice to recover a neutrinolike fluid behavior in the appropriate limit. The choice from [19] maintains this behavior with a slight change to allow the crossing of $w = 0$. In our notation, this relation becomes

$$\dot{\sigma}_g = -3\mathcal{H}\sigma + \frac{8k^2}{3(1 + w)}c_v^2\hat{\Theta}_g,$$

$$\text{with} \quad \hat{\Theta} = \theta/k^2 - \zeta - \frac{1}{2}\dot{\nu}, \qquad (7)$$

where ν and ζ are scalar perturbations of the metric,[1] contributing as the time-space component $-\nabla_i\zeta$ and the traceless space-space component $(\nabla_i\nabla_j - \frac{1}{3}\gamma_{ij}\nabla^2)\nu$. The variable c_v^2 is a free parameter of the model and is similar to shear viscosity in fluid dynamics; see Sec. IV. A of [19] for more details on this connection. The gaugeinvariant

variable $\hat{\Theta}$ reduces to the velocity perturbation in the conformal Newtonian gauge where the last two terms vanish. One recovers free-streaming massless neutrinos truncated at the quadrupolar moment by setting $w = c_s^2 = c_v^2 = \frac{1}{3}$.

In full generality, the parameters of GDM can take a functional form of $w(a)$, $c_s^2(a, k)$, and $c_v^2(a, k)$. However, our analysis restricts the latter two to constants, given that the freedom in $w(a)$ is already sufficient to draw conclusions about the exploration of such high-dimensional models.

B. Numerical implementation

We now discuss our implementation of our model of GDM via modification of the publicly available Einstein-Boltzmann solver CLASS [26].

First, we discuss our choices of parameters to describe the model. Traditionally energy density is set by the fraction of energy density today Ω_g. However, the flexibility in the history of $w(z)$ can make setting an appropriate range difficult. Instead, we pick a redshift of interest z_g at which we set the fractional contribution of GDM $f_{\rm gdm} \equiv \rho_g(z_g)/(\rho_r(z_g) + \rho_m(z_g) + \rho_g(z_g))$. When z_g is large enough so that dark energy does not play a significant role, $f_{\rm gdm}$ is a good approximation of the fraction of the energy density that GDM provides at z_g. We keep the other components of the ΛCDM model exactly the same, treating the GDM as an *additional* component. However, we have to respect the budget equation that requires all energy fractions Ω_x of the various species x to satisfy $\sum_x \Omega_x = 1$. Since we are adding some small $\Omega_g > 0$ we have to subtract some small amount from some other component, and we choose the dark energy (in our case in the form of a cosmological constant) for that. In most considered cases (which have $w > 0$ at late times) the change in Ω_Λ caused by this is negligible since $\Omega_g \ll 1$. Only for the validation test in Sec. II C do we have a non-negligible Ω_g, which we subtract from Ω_Λ to keep $\sum_x \Omega_x = 1$. To compute Ω_g we numerically integrate ρ_g forward in time.

The history of $w(z)$ is determined by a set of N pairs of control points $(\log_{10}(a_1), w_1)\dots\log_{10}(a_N), w_N)$. Between points, we implemented piecewise linear interpolation. We used logarithmic space rather than linear to give finer control in any decade. This interpolation is a simple way to describe a continuous function without needing additional guards to enforce the physical requirement that $-1 \leq w \leq 1$ even between control points, which can plague smoother interpolation schemes.[2]

---

[1]These are often also denoted as $B \equiv \zeta$ (scalar potential of time shift vector) or $E \equiv H_L \equiv \nu$ (scalar potential for the traceless part of the spatial metric) [21–25].

[2]The largest drawback in our choice is that c_a^2 will not be continuous as it involves $\dot{w}$. If continuity of c_a^2 were important for some application, other choices are possible such as a cubic piecewise monotonic spline which enforces monotonicity between control points.

Valid inputs of control points must range from when CLASS initializes the background, $a_{\text{ini}} = 10^{-14}$ by default, to today. To ensure radiation domination for initial conditions, we set the restriction that $w \leq 1/3$ at early times. The Appendix derives the initial conditions. We denote this realization of GDM with complete freedom over the $w(a)$ evolution through a multitude of control points as HDGDM.

At points within CLASS, we must choose a decomposition of energy density sources into radiation and pressureless matter.[3] However, there is no singular way to divide ρ_g into materials of a constant equation of state parameter. Our choice splits GDM into two materials depending on the value of w. We divide up the range of w into intervals with endpoints $(-1, 0, 1/3, 1)$ corresponding to dark energy, nonrelativistic matter, radiation, and a free scalar field, respectively. For a w contained in interval (w_I, w_J), we divide ρ_g into

$$\rho_{I,\text{g}} = \frac{w - w_J}{w_I - w_J} \rho_{\text{g}} \quad \text{and} \quad \rho_{J,\text{g}} = \rho_{\text{g}} - \rho_{I,\text{g}}. \quad (8)$$

This decomposition ensures that each component is nonnegative and is continuous in the transition between intervals.[4]

As described above, c_s^2 and c_v^2 are additional free parameters affecting the evolution of the perturbations. Both perturbation parameters lie in the range $[0, 1]$ in order to support growing modes and to have characteristic scales grow at subluminal rates. Our current implementation has these parameters as constants in time. By default, if the user does not set c_s^2, then NAP is turned off, forcing $c_s^2 = c_a^2$.

C. Numerical validation of the GDM implementation

Generalized dark matter is a very general material that can mimic many other materials already implemented in CLASS. We first compare against perfect fluids of constant equation of state parameter less than 0 before looking at one that linearly varies with scale factor. Subsequently, additional neutrinos and "self-interacting dark radiation" (SIDR) with $w = 1/3$ with and without free streaming, respectively, are modeled. Our CLASS implementation can reproduce the temperature, polarization and lensing (TT, TE, EE, $\phi\phi$) power spectra for all the test cases discussed below to within a precision goal of 0.1% of cosmic variance for $\ell < 4000$, sufficient for our applications.

CLASS already has an implementation of a nonperfect fluid (FL). It must have a time-varying equation of state

---

[3]This is important, for example, when CLASS sets values consistent with big bang nucleosynthesis of the helium abundance, or computes small corrections to the initial conditions. The overall impact on observables is rather minor, though.

[4]This decomposition also recovers the usual neutrino splitting as $\rho_r \approx 3P_\nu$ and $\rho_m \approx \rho_\nu - 3P_\nu$ that is used in CLASS.

parameter of the $w_{\text{fl}}(a) = w_0 + w_a(1 - a/a_0)$ under the restrictions that $-1 < w(a_{\text{ini}}) < 0$ [with $w(a_{\text{ini}}) \approx w_0 + w_a$]. These fluids serve as a helpful place to start comparisons.

We first validate with $w_{\text{fl}}(a) = w_0$ (explicitly setting $w_a = 0$). For the HDGDM we set $w = w_0$ at initial and final times with no viscosity or NAP. To stay reasonably close to the observed data, we set $\Omega_{\text{g}} = \Omega_{\text{fl}} = 0.1$ while keeping all other parameters to their default values in CLASS. Due to the strict bounds for $w_0 + w_a$ we compare against $w_0 = \{-1/10, -1/3, -2/3, -9/10\}$. The resulting spectra agree to within our 0.1% goal.

By allowing w_a to be nonzero, we can make an additional comparison. Due to the different functional forms for time dependence, FL's linear function in a can only be approximately described by the piecewise linear $w(\log a)$ of HDGDM. We use 249 control points with increasing density as a tends to 1 and manage to achieve our target accuracy. We compare these fluids at all combinations of $w(a_{\text{ini}})$ and w_0 drawn from $\{-1/10, -1/3, -2/3, -9/10\}$ with all other parameters treated the same as above, and find excellent agreement.

Comparison for materials with $w(a_{\text{ini}}) > 0$ can also be made by attempting to mimic the behaviors of neutrinos or SIDR. By design, the shear stress of GDM recovers the same behavior as the truncated neutrino hierarchy when $c_v^2 = 1/3$. For the best comparison, we set the fluid approximation of CLASS to match Hu's formalism [3]. To set the energy contribution, we contrast between an increase in the effective number of neutrino species (N_{ur}) by 10% and the equivalent Ω_g while setting $w = 1/3$ for all time. Similarly, by turning c_v^2 off and replacing the additional N_{ur} with N_{idr} (effective number of neutrino species that are self-interacting), we can subsequently reproduce the spectra of SIDR within our precision goal.

We conclude that our realization of GDM in CLASS allows for a robust modeling of a wide variety of equations of state to high precision. While execution times of the specific implementations of specialized materials (such as FLD or N_{ur}) can outperform our generalized implementation of GDM in their specific domains, the ability to seamlessly transition from one material to another has otherwise been impossible. Subsequently, we leverage this capability to search for models satisfying cosmological data while bringing concordance to the observed tensions.

III. MODEL SPACE EXPLORATION

The traditional approach for exploring the implications of a model space and a given dataset is to calculate the posterior probability distribution of the model parameters given the data and visually examine one- and two-dimensional marginal posterior distributions. Here we emphasize that applying such methodology to relatively high-dimensional spaces can lead to unusual and undesirable results. For example, one might naively think that

broadening a model space by introducing additional para-
metric degrees of freedom or relaxing priors on these
degrees of freedom would necessarily lead to broader
distributions of parameters of interest, such as the marginal
posterior distribution of H_0. The breadth of the prior, and
in particular its level of support for H_0 values of, say,
73 km/s/Mpc, would then indicate how well the model
space in question can accommodate a high H_0 value. We
have found, though, that this is not always the case. In fact,
we have found that narrowing the parameter space of a
model to a subspace that contains regions that admit good
fits to the combined CMB and SH0ES data can never-
theless lead to a *wider* marginal H_0 distribution compared
to the original. This effect has been noted in lower-
dimensional cases before, such as in [6,13] where it had
a marginal impact. However, in the high-dimensional broad
HDGDM parameter space this prior volume effect is
qualitatively more important (see Fig. 1).

This section presents a worked example in which we can
observe and understand the cause of this unusual feature of
the traditional investigation. The emergence of this unde-
sirable result—of interesting solutions becoming effec-
tively lost—leads us to examine how the traditional
approach is not suited for us, given our particular goals
for exploring the implications of data. Although our
primary goal in this section, and with this paper, is to
point out the pitfalls of high-dimensional model space
exploration, we briefly discuss what one can do instead.
Finally, we include some takeaways from our investigations
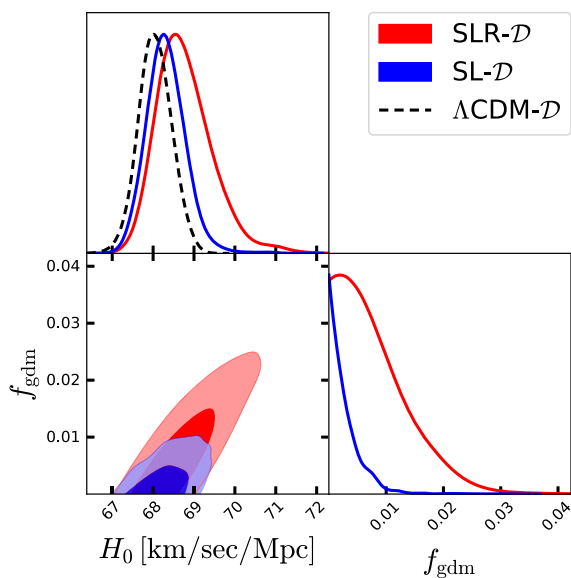that we can manage to make despite the pitfalls we are
emphasizing.

FIG. 1. Triangle contour plot of H_0 and f_{gdm} for the steplike
(SL) model and the steplike (restricted) (SLR) model with dataset
$\mathcal{D}$ (see text for definitions). The shaded regions indicate the 68%
and 95% credible regions.

A. Standard techniques

We begin using HDGDM to explore a parameter space
we knew beforehand contained an interesting solution to the
H_0 tension. In particular, we choose as a motivating model
"Wess-Zumino dark radiation" explored in [10,13,27].

Models like Wess-Zumino dark radiation and potentially
other near radiationlike fluids introduce light particles with
a decay channel into massless particles. The combined
system of particles starts with an equation of state $w = 1/3$,
which decreases as the particles' rest mass energy becomes
significant compared to the thermal energy of the particles,
after which only the massless species remains and the
equation of state returns to $w = 1/3$.

Our toy version of these models is HDGDM with $w =
1/3$ for times before $a = 10^{-5}$ and after $a = 10^{-2}$. We
include five equation-of-state parameters $\{w_1, w_2, \ldots w_5\}$ at
scale factors $\{10^{-4.5}, 10^{-4}, \ldots 10^{-2.5}\}$ respectively. For a
preliminary investigation, we turn off NAP and viscosity
and set uniform priors over $[-1, 1]$ for w_i and $[0, 0.7]$
in f_{gdm} at $z_g = 3000$. We denote the cosmological model
formed by ΛCDM extended by this parametrization of
HDGDM as "steplike".

For all models explored and the baseline ΛCDM model,
we adopt flat priors over standard cosmological parameters
$\{H_0, \omega_b, \omega_c, \ln(10^{10}A_s), n_s, z_{\text{reio}}\}$. The neutrino sector
assumes one massive, $m_\nu = 0.06$ eV, and two massless
species (following [28]). We use the "halofit" module of
CLASS to include nonlinear effects.

Following standard approaches for model evaluation, we
produce the posterior distribution via the Polychord algo-
rithm inside of Cobaya [29,30]. We combine several
datasets into the collection, $\mathcal{D}$, which includes data from
Planck, baryon acoustic oscillation (BAO) measurements,
and Pantheon. In particular, we make use of Planck 2018
TT, TE, EE for low and high ℓ modes (marginalized
over the nuisance parameters) as well as the lensing
reconstruction [31,32]. BAO measurement data is taken
from BOSS DR12 [33], 6dF [34] and MGS [35]. Lastly,
we include Pantheon supernova data [36].

We show some of the posteriors of the steplike model in
Fig. 1. One might initially conclude that there is minimal
support for substantial f_{gdm} values and, by extension,
GDM; however, this conclusion would be a questionable
one as the result is highly dependent on the implicitly
assumed priors (as we will soon see) and the priors are
chosen in some sense arbitrarily. The posterior that we
calculate is only the posterior *given* these priors: that the
model is correct (at some point in the parameter space)
and that the probability (prior to examining any data) is
distributed uniformly across the parameter space. These
priors do not reflect our true prior beliefs about this model
space, one we are only adopting for phenomenological
exploration.

We show the marginalized posteriors of the w_i in Fig. 2.
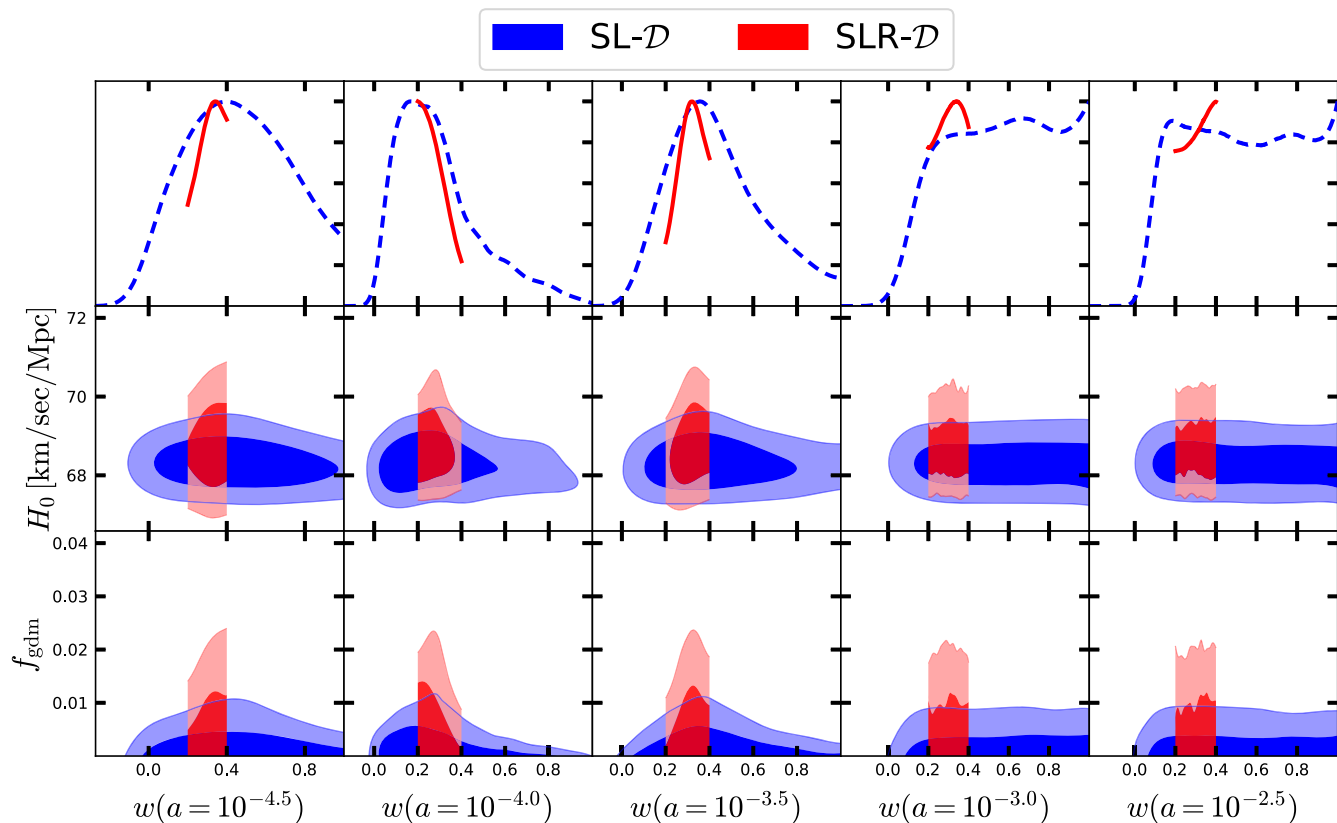Here we observe a band of values in the earliest three w_i,

FIG. 2.   The posterior of each w_i parameter of steplike and steplike (restricted) models along with their contours in relation to H_0 and f_{gdm} using the $\mathcal{D}$ data collection. The shaded regions indicate the 68% and 95% credible regions.

which both support larger f_{gdm} and coincide with preferred values of w_i. This observation motivates a "steplike (restricted)" model where w_i are all restricted to a uniform prior from [0.2, 0.4]. This choice narrows the steplike model closer to behaviors seen in models like Wess-Zumino dark radiation, where we expect typical w values to fall in the [0.25, 0.33] range. Figures 1 and 2 show the resulting posterior in terms of H_0 and the model parameters.

We see much higher values of f_{gdm} now contained in the 95% credible region. More interesting is the impact on the distribution of H_0. While we expect an upward shift in peak probability, given the increased amount of the HDGDM, the broadening of the distribution is a surprise. When going from steplike to steplike (restricted), we have narrowed our priors of each w_i and thus narrowed the total prior parameter space (reducing the prior uncertainty). This restriction has effectively added information, yet we see less certainty in the posterior of H_0.

We attribute the change in predictions to a volume effect. In the steplike model, when f_{gdm} tends to zero, any impact of GDM is minimal, reducing the model to effectively ΛCDM. As a result, the marginalized distribution for H_0 gets uniform contributions from the whole of the w_i parameter space. As we increase f_{gdm}, only the $w(z)$

histories producing outputs that fit data well find significant weight. Naturally, these permitted histories take up a small portion of all possible values in w_i. In the steplike (restricted) model, we have reduced the w_i parameter space's total volume increasing the ratio of supported volume to prior volume. Thus the volume effect has a diminished boost when $f_{\mathrm{gdm}} \approx 0$. Furthermore, the remaining region contains histories that can fit data well, allowing f_{gdm} to find support above zero. Thus, we see that looking primarily at the posterior region of support might cause premature conclusions on the existence of viable regions within the steplike model away from ΛCDM.

The failure of standard inference methods to distinctly pick out the potentially interesting area of model space raises the question if it is the correct choice for our purposes. When conducting parameter estimation, using marginalized distributions is a natural choice. In contrast, our observations in this section call for alternative methods when seeking a region to focus on in large model spaces which can be sensitive to prior assumptions. We now review a few of those techniques.

B. Model searching techniques

The peculiarities between steplike and steplike (restricted) cue us to examine our goals and methods.

The fact that we are searching for a submodel rather than estimating parameters is critical here. Marginalized posteriors, vital to the latter, can mislead us in the former. We briefly discuss other tools helpful in finding new models of interest. To begin, we present the technique we used (minimizing the log-likelihood via simulated annealing) before suggesting potential alternatives for other problems.

Approaches which look for parameters that provide good fits to data are particularly relevant to our goals. We can easily discard a model that has no improvement in quality of fit when compared to ΛCDM. If a notable region can provide good fits, then features of that region could be extracted to motivate theoretical models. Thus, relevant techniques must find the existence and location of these regions.

An important tool to discover potential subspaces or validate choices made for other reasons is χ^2 minimization. However, the curse of dimensionality of the HDGDM model has proven to make such a search challenging. Even our relatively small dimensional extension steplike has many local minima. Additionally, parameters like the last two w_i parameters and their near-flat posterior may also have weak (and potentially noisy) relations to data. Either of these problems may cause standard minimizing algorithms to have issues. We have found that simulated annealing has had the most success though not without the need for care.

In practice, we start searches with several independent Markov chains, which may originate in widely separated initial points. We then seed a second collection of chains with initialized parameters drawn from a normal distribution centered at the best fit of the first set. We examine the second collection of chains to ensure no wide swings in the best-fit parameter values. Interestingly, most of our primary collection of steplike chains ends inside the steplike (restricted) region, with the overall best fit of the secondary run not far from this region.

More advanced minimization techniques based on annealing are currently being developed, and can be compared to other robust minimization approaches such as [37,38].[5]

Although we do not use it here, likelihood profiling, as done for example in [40], can also be a helpful tool to see how the best fit of a model evolves as we vary a parameter of interest. Given that there is no prior weighting in likelihood profiling, this will naturally outline parameter regions of good fit, as long as good convergence of the profiler is ensured.

Another model search technique returns to Markov chain Monte Carlo (MCMC) methods. One could use the result of these chains with some threshold cutoff in log-likelihood to locate localized regions of parameter space which provide good quality fits. In contrast to traditional techniques, the
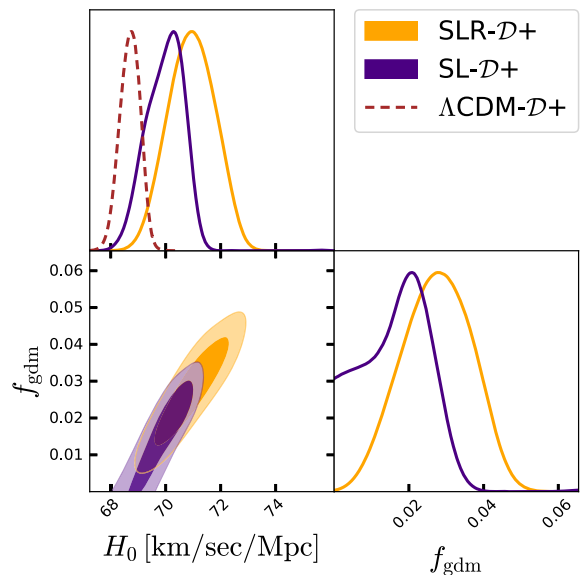

FIG. 3. Triangle contour plot of H_0 and $f_{\rm gdm}$ for the SL model and the SLR model with the dataset $\mathcal{D}+$ (see text for definitions). The shaded regions indicate the 68% and 95% credible regions.

focus on the quality of fit rather than the marginalized posterior will get around potential volume effects. This search could be aided by changing the temperature of the MCMC as well; by making the chain run colder one would further emphasize regions of good fit.

C. Hubble constant prior

In this subsection, we extract additional insights from steplike (restricted), including its flexibility when attempting to fit additional data and what difference we see from our original motivating model. We will see that solutions exist within the model that bring concordance across CMB anisotropies, the Cepheid and supernova based distance ladder, and BAO data.

We first explore an expanded dataset collection, $\mathcal{D}+$, which adds SH0ES data to our original collection [17]. We see some preliminary results in Figs. 3 and 4. Adding SH0ES lowers the quality of fit ΛCDM can provide while $f_{\rm gdm}$ is small. Thus, the volume effect boost is diminished even in the steplike model. Furthermore, once we move from steplike to steplike (restricted), there is a clear preference for $f_{\rm gdm} > 0$, with $f_{\rm gdm}$ shifting from $f_{\rm gdm} < 0.030$ (95% CL) to $f_{\rm gdm} = 0.028 \pm 0.0098$, and a corresponding 1-$\sigma$ shift in H_0 from 70.0 ± 0.7 km/s/Mpc to 70.9 ± 0.8 km/s/Mpc. These constraints can also be compared to the posterior without the addition of the SH0ES prior, which is at only $H_0 = 68.3 \pm 0.5$ km/s/Mpc for the steplike model. An interesting consideration to draw from this is that in order to check the validity of a given model in terms of easing a particular tension, it can be extremely helpful to force it into the beneficial parameter space by including the additional data.
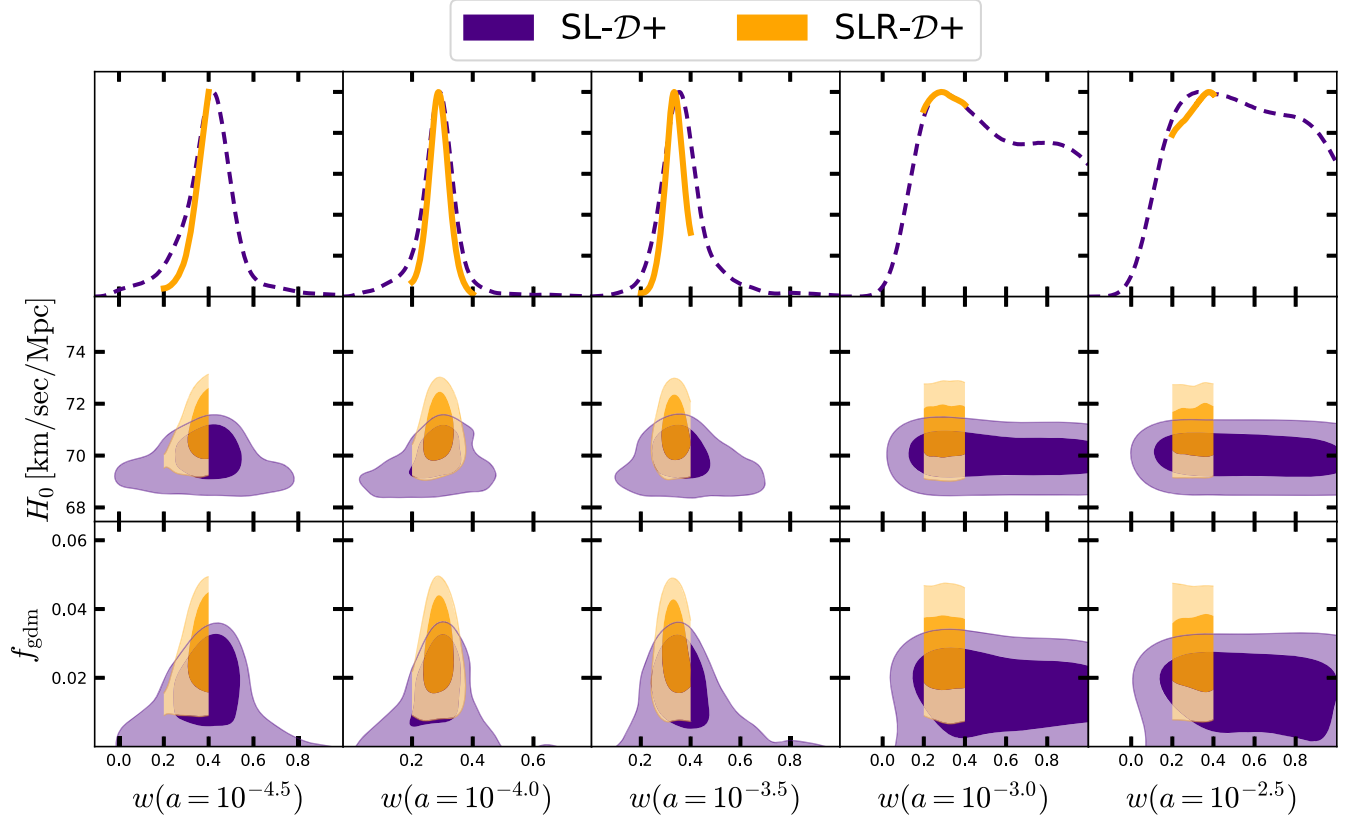
---

[5]We note that simplex-based methods like [39] would typically be far too slow in such high-dimensional parameter spaces.

FIG. 4.   The posterior of each w_i parameter of (SL) and (SLR) models along with their contours in relation to H_0 and f_{gdm} using the $\mathcal{D}+$ data collection (see text for definitions). The shaded regions indicate the 68% and 95% credible regions.

We note that under $\mathcal{D}+$, the posterior of w_1 at $a = 10^{-4.5}$ is cut off by the steplike (restricted) prior. However, even given an extended range up to 0.6 in w_1 the properties of the model are not significantly different, so for brevity, we do not introduce another model. However, this may hint that something of interest lies in the $w > 1/3$ range, a region inaccessible to most light particle models.

To get a better understanding of the properties of the models, we examine their respective best fits. In our explorations of these spaces, all sampled parameters have flat priors except for A_{planck} of the Planck dataset, which has a normal distribution. Thus for a fair comparison, we consider the sum of $\Delta\chi^2$ for each dataset along with twice the negative of the log prior of A_{planck}, discarding any other priors as they provide only constant effect within their respective models. The results can be seen in Table I, where

it becomes clear that despite the smaller space, the best fit of the restricted model is very close in quality of the best fit over the larger space. In contrast to ΛCDM the search demonstrates that better fits to SH0ES data exist while improving the fit to Planck data. The most significant pushback to the new parameters comes not from Planck but from BAO data.

This better fit can also be seen through the Q_{DMAP} criterion introduced in [41]. In our case, we obtain a Q_{DMAP}-based Hubble tension of 4.7σ in ΛCDM, while in the steplike model we obtain only 2.6σ and in the steplike (restricted) model 2.7σ. These Q_{DMAP} show (by definition) the expected ordering that the models with more restricted parameter spaces perform worse. In particular, the ability of the HDGDM extension to ease the Hubble tension in some part of the large parameter space becomes

TABLE I.   Change in χ^2 values in comparison to the ΛCDM best fit of the same dataset. The acronym SL represents the steplike model, while SLR represents the steplike (restricted) model. We also show the shift in the H_0 and S_8 best-fit values.

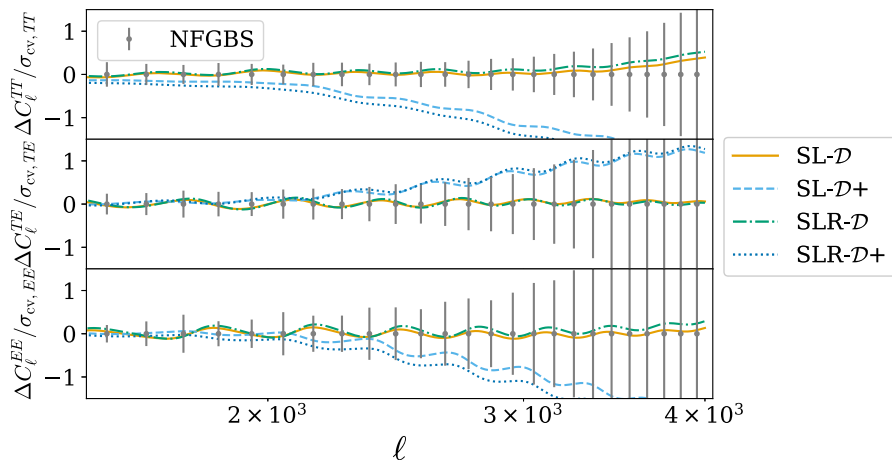| Dataset	Model	$\Delta\chi^2_{\mathrm{CMB}}$	$\Delta\chi^2_{\mathrm{BAO}}$	$\Delta\chi^2_{\mathrm{SN}}$	$\Delta\chi^2_{\mathrm{SH0ES}}$	$-\Delta 2 \ln \pi(A_{\mathrm{planck}})$	Total	H_0 (Km/s/Mpc)	ΔH_0	S_8	ΔS_8
$\mathcal{D}$	SL	-1.33	0.20	-0.01		-0.05	-1.19	68.38	0.32	0.837	0.007
$\mathcal{D}$	SLR	-1.32	0.20	-0.02		0.03	-1.11	68.67	0.56	0.836	0.006
$\mathcal{D}+$	SL	-0.74	0.45	0.00	-15.67	-0.11	-16.07	71.66	2.96	0.829	0.012
$\mathcal{D}+$	SLR	-0.38	1.07	0.02	-16.20	-0.15	-15.63	71.88	3.18	0.829	0.012

FIG. 5. Best-fit power spectra for each model and data collection, with the fiducial ΛCDM best fit to $\mathcal{D}$ spectrum subtracted, divided by the cosmic variance of the same fiducial. The error bars are a forecast of near-future ground based survey (NFGBS).
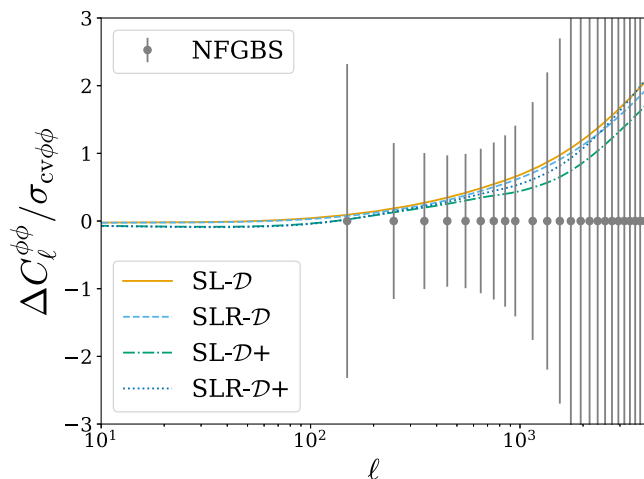

FIG. 6. Best-fit lensing ($\phi\phi$) power spectra for each model and data collection, with the fiducial ΛCDM best fit to $\mathcal{D}$ spectrum subtracted, divided by the cosmic variance of the same fiducial. The error bars are a forecast of near-future ground based survey (NFGBS).

far more evident using Q_{DMAP} as the metric and is not overshadowed by prior volume effects.[6] Thus the Q_{DMAP} criterion can be used as a fast and relatively cheap check to see if further exploration of the model parameter space might be sensible.

D. Noteworthy features

An ideal outcome of this work would be to inspire the creation of a physical model with features found in our steplike model, which can make predictions that are distinguishable from ΛCDM using future observations. We begin by considering the spectra of the best-fit parameters to establish how they differ from ΛCDM. Subsequently, we consider what typical histories of $w(z)$ and $H(z)$ a physical steplike model might contain. We finally consider if there are any implications for S_8 tensions.

We compare the best fits of steplike and steplike (restricted) to ΛCDM, in Figs. 5 and 6. In these plots, we compare the change of the respective spectra as a fraction of cosmic variance. For a relevant scale we provide forecasted error bars of a 10 000 square degree survey reaching a depth of 9 μK-arcmin in temperature and 12 μK-arcmin in polarization, which we refer to as near-future ground based survey (NFGBS). Such a survey could be conducted in the next few years with existing instruments, such as SPT-3G [42].

Without SH0ES data, the steplike and steplike (restricted) best-fit spectra differ very little from the ΛCDM best fit. The most significant difference is increased power of the $\phi\phi$ and TT spectra at small scales.[7]

With SH0ES, the effect on the TT, TE, EE spectra becomes more pronounced, causing changes in TT that should be detectable with upcoming observations. All models considered fit the current spectral data well but have potentially divergent behaviors at ℓ values beyond current data. We consider the ability of NFGBS (see above) for $\ell \leq 4000$ to distinguish our models from ΛCDM. The combined signal to noise ratios of the (TT, TE, EE, $\phi\phi$)

---

[6]This, of course, does not imply that the HDGDM extension is a particularly useful model, based on its mostly phenomenological construction. Indeed, its Aikaike information criterion $\chi^2 + 2N_{\text{param}}$ shows an overall difference of 10.9 without the Hubble prior (and -4 with the Hubble prior) due to the large parameter penalty, thus being easily outperformed by other smaller models. However, it does imply that the HDGDM can indeed be used as a valuable tool to aid in the search for mechanisms of reconciling the tension.

[7]We note that this increase in lensing power is primarily driven by differences in the $\Omega_m h^2$ best fit from the CMB anisotropy data allowed by the additional HDGDM, while the direct impact of the HDGDM on the CMB lensing is instead very minute.
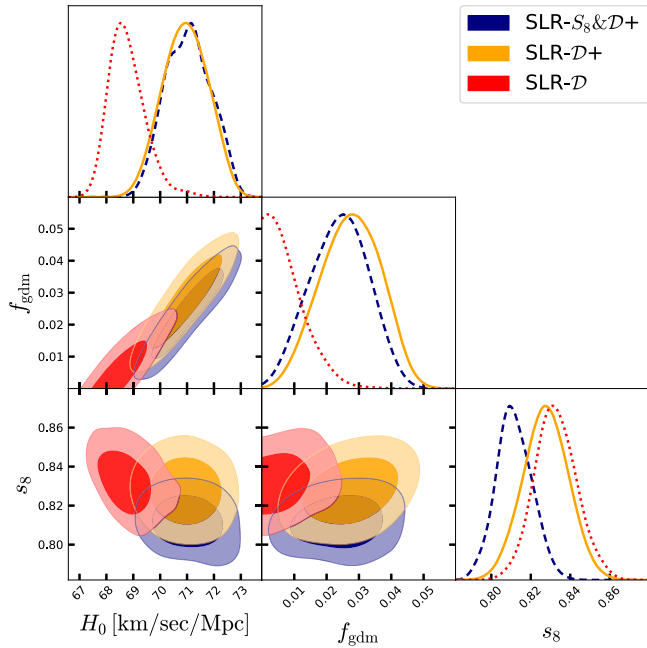
FIG. 7. A comparison of the SLR posterior with the $\mathcal{D}$, $\mathcal{D}+$ and S_8 & $\mathcal{D}+$ data collections (see text for definitions). The shaded regions indicate the 68% and 95% credible regions.

spectra are found to be 2.5 for the steplike model with $\mathcal{D}$ [2.6 for the steplike (restricted) model] and 11.0 with $\mathcal{D}+$ for the steplike model [13.5 for the steplike (restricted) model] with the lensing reconstruction being the largest contributor to former and the temperature anisotropies

overtaking for the latter. We thus expect near-future data to be capable of discriminating between the best-fit solutions of ΛCDM and the steplike (restricted) model over the $\mathcal{D}+$ data collection.

In Fig. 8, we show preferred histories of $w(z)$ and $H(z)$. The plot presents the Hubble parameter as a fractional change from the fiducial values of the best-fit value of ΛCDM on the $\mathcal{D}$ data collection.

Overall the $\mathcal{D}$ dataset does not constrain $w(z)$ particularly well, with only a minor trend to lower $w(z)$ at $z \sim 10^4$ and a return upwards for the next node at $z \sim 10^{3.5}$. Nevertheless, the mean shape does resemble the behaviors of [10]. With the addition of SH0ES data $f_{\rm gdm}$ is larger and thus HDGDM has an increased impact. Thus, the history of $w(z)$ has more impact on the observables. The three control points before $z = 10^3$ become more constrained, with the latter two points about as free as before. These constraints reinforce how the epoch leading up to matter radiation equality and recombination can most impact predictions and, consequently, how sensitive data are to these parameters. Particularly interesting are the features of a large spike of $w > 1/3$ at $z \sim 10^{4.5}$ and a dip at $z \sim 10^4$. While the latter is known in the context of Wess-Zumino dark radiation, the former is quite interesting as a starting point for potential future exploration of mechanisms easing the Hubble tension. We leave a more detailed investigation of this spike feature to future work. Even when focusing on the mean behavior, we see that steplike (restricted) can make a significant shift of H_0 without extreme spikes or dips, supporting the idea that the restricted model space still has more than enough flexibility to fit $\mathcal{D}$ data while
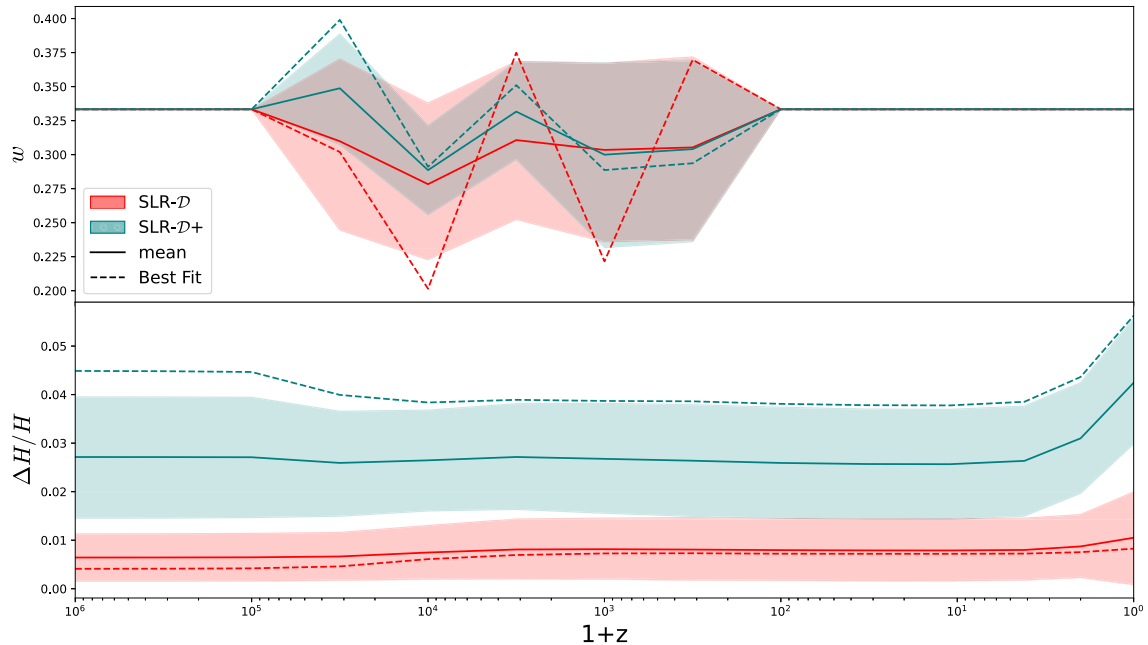

FIG. 8. The history of $w(z)$ and the fractional change in the history of $H(z)$ from the fiducial ΛCDM best fit for the steplike (restricted) model. The shaded region indicates the 68% credible region.

relieving tension with SH0ES observations. In contrast, even with the freedom that HDGDM provides, the Hubble expansion histories do not seem to broaden significantly, with the 1σ upper bound of the steplike (restricted) case only being about 1% (resp. 4%) larger than in the ΛCDM fiducial for $\mathcal{D}$ (resp. $\mathcal{D}+$). However, as before, these bounds should not be misinterpreted. They represent the marginalized preference of histories of $H(z)$ for a given model with particular priors, but are not to be seen as solely data-driven bounds on possible deviations in expansion histories. Indeed, this is why the contours for the two models can disagree for the same dataset at the $\sim 1\sigma$ level.

In another line of inquiry, we see intriguing implications when we look at the impact of S_8. Unlike many models proposed in the literature to ease the Hubble tension, there is room within the HDGDM extension to increase H_0 without increasing S_8. Figure 7 supports this idea. In the plot, we post process[8] the results of $\mathcal{D}+$ with a prior from DES3 of $S_8 = 0.776 \pm 0.017$ [43]. The figure shows that S_8 and H_0 are uncorrelated (or even slightly negatively correlated before SH0ES data is added). This is supported by the best-fit values, which suggest that the steplike (restricted) model can fit all the data in $\mathcal{D}+$ without increasing the S_8 tension.

IV. CONCLUSIONS

We have implemented and explored a high-dimensional generalized dark matter (HDGDM) model with a free equation of state $w(a)$. We demonstrated that this model can mimic various cosmological fluids, including models of interest such as typical self-interacting dark radiation species. We applied this formalism to mimic a stepped dark radiation fluid and investigated the constraints of this steplike model.

We showed that the marginalized posterior intervals are dominated by prior volume effects, leading to potentially rather misleading conclusions about the model viability. In particular, we showed that a more restricted version of the model has a much wider range of allowed values for H_0 than the unrestricted steplike model. Despite adding information through this restriction, the uncertainty on the inferred H_0 increases. This serves as a cautionary tail against using the credible intervals of parameters for model selection or even for the search for viable parameter space within a given model.

We have discussed several ways of circumventing these issues, such as using techniques based on minimization or likelihood cutoffs. This also leads us to the conclusion that the Q_{DMAP} criterion of [41] is an excellent indicator of whether such prior effects are at play. Indeed, another option of estimating whether a model might be useful (or contain a useful subspace of parameters) is to subject it to more challenging data that can direct to a relevant novel region of interest.

By adding a prior on the Hubble constant, for example, we can force the steplike and restricted step-like models into a regime where the nontrivial freedom in $w(a)$ can be used more effectively. Indeed, we observe interesting features in the equation of state (a spike at $z \sim 10^{4.5}$ and a dip at $z \sim 10^4$) that motivate future investigation. Furthermore, we show that future data should be capable of either constraining the ability of the HDGDM extensions to ease the Hubble tension or potentially detecting signatures that differ from ΛCDM.

We expect the development of fast and robust minimization techniques to aid the community in avoiding misleading conclusions based on marginalized posterior distributions, and stress that the validity of a model should be more robustly assessed. The HDGDM presented in this work serves as a prime example, displaying interesting features which might have otherwise been overlooked and certainly motivate further investigation.

APPENDIX: INITIAL CONDITIONS

To initialize the perturbation variables the asymptotic behavior of the evolution equations is examined. The needed equations are $A1(a-1)$ of [19].[9] Differing from their approach, set the ansatz of the scale factor to take the form $a = a_i \mathcal{H}_i \tau \sum_{p,q} a_{p,q} (\epsilon_m \tau)^p (\epsilon_g \tau^\beta)^q$, where $\beta = 1 - 3w_{g,i}$ and $\epsilon_I = \frac{\rho_{I,i}}{\rho_{r,i}}$ for matter and GDM and $3\mathcal{H}_i^2 = 8\pi G \rho_{r,i} \cdot a_i^2$ is the conformal expansion rate to zeroth order in matter and GDM. All i subscripts denote the quantities at initial conditions which are assumed to be deep enough in radiation domination to expect ϵ_I to be small. The treatment assumes that w_g is slowly varying at this time period, enough to ignore its evolution while setting initial conditions. The choice of ansatz easily accommodates limiting cases where matter or GDM are turned off. The metric and materials perturbation variables are expresses in powers of $x = k\tau$. Unfortunately they do not lend themselves to a series in powers of $(\epsilon_m x), (\epsilon_g x^\beta)$ with a finite polynomial in

---

[8]We use importance sampling to add the effect of the S_8 prior.

[9]The notation of [20] is used, which differs from [19] and can be converted using $\theta_k = \theta_{\text{MB}}/k^2$ and $\Sigma = \frac{3}{2}\sigma_{\text{MB}}$.

x at zeroth order. Instead we express in a series of powers of x and x^β which moves the dependence of ϵ_g, ϵ_m into the coefficients while admitting the pure radiation solution if desired. The fraction of radiation density that is neutrinos is denoted $S_\nu = \rho_\nu/\rho_r$. After using rescaling to set $\eta(x = 0) = 1$ (used in CLASS) the leading order solutions in small x then become

$$a = a_i \mathcal{H}_i \tau \left(1 + \frac{\mathcal{H}_i \tau}{4} \epsilon_m + \frac{(\mathcal{H}_i \tau)^\beta}{2(1+\beta)} \epsilon_g \right), \quad \text{(A1)}$$

$$\eta = 1 - \frac{5 + 4S_\nu}{12(15 + 4S_\nu)} x^2, \quad \text{(A2)}$$

$$h = \frac{1}{2} x^2, \quad \text{(A3)}$$

for the scale factor and the metric potentials, and

$$\delta_\gamma = \delta_\nu = \frac{4}{3} \delta_b = \frac{4}{3} \delta_c = \frac{-1}{3} x^2, \quad \text{(A4)}$$

as well as

$$\delta_\nu = \frac{-k(23 + 4S_\nu)}{36(15 + 4S_\nu)} x^3, \quad \text{(A5)}$$

$$\delta_g = -\frac{(1+w)(1 - \frac{3}{4} c_s^2) + 12 c_v^2 \frac{c_s^2 - w}{(15 + 4S_\nu)}}{4 + 3c_s^2 - 6w} x^2, \quad \text{(A6)}$$

for the overdensities and

$$\theta_\gamma = \theta_b = \frac{-k}{36} x^3, \quad \text{(A7)}$$

$$\theta_g = \frac{-k}{4 + 3c_s^2 - 6w} \left(\frac{c_s^2}{4} + \frac{4c_v^2(2 - 3(w - c_s^2))}{3(15 + 4S_\nu)(1+w)} \right) x^3, \quad \text{(A8)}$$

for the velocities and finally

$$\sigma_\nu = \frac{2x^2}{3(15 + 4S_\nu)}, \quad \text{(A9)}$$

$$\sigma_g = \frac{8c_v^2 x^2}{3(15 + 4S_\nu)(1+w)}, \quad \text{(A10)}$$

for the shear terms. These relations agree with [19,44] when w, c_s^2, c_v^2 are kept to first order and when $c_v^2 = 0$ respectively.

[1] W. Hu and M. J. White, Astrophys. J. **479,** 568 (1997).
[2] L. Knox and M. Millea, Phys. Rev. D **101,** 043533 (2020).
[3] W. Hu, Astrophys. J. **506,** 485 (1998).
[4] V. Poulin, T. L. Smith, T. Karwal, and M. Kamionkowski, Phys. Rev. Lett. **122,** 221301 (2019).
[5] P. Agrawal, F.-Y. Cyr-Racine, D. Pinner, and L. Randall, Phys. Dark Universe **42,** 101347 (2023).
[6] T. L. Smith, V. Poulin, J. L. Bernal, K. K. Boddy, M. Kamionkowski, and R. Murgia, Phys. Rev. D **103,** 123542 (2021).
[7] J. C. Hill, E. McDonough, M. W. Toomey, and S. Alexander, Phys. Rev. D **102,** 043507 (2020).
[8] R. Murgia, G. F. Abellán, and V. Poulin, Phys. Rev. D **103,** 063502 (2021).
[9] F. Niedermann and M. S. Sloth, Phys. Rev. D **102,** 063527 (2020).
[10] D. Aloni, A. Berlin, M. Joseph, M. Schmaltz, and N. Weiner, Phys. Rev. D **105,** 123516 (2022).
[11] V. Poulin, T. L. Smith, and T. Karwal, arXiv:2302.09032.
[12] L. Hart and J. Chluba, Mon. Not. R. Astron. Soc. **519,** 3664 (2023).
[13] N. Schöneberg and G. Franco Abellán, J. Cosmol. Astropart. Phys. 12 (2022) 001.
[14] A. Hojjati, E. V. Linder, and J. Samsing, Phys. Rev. Lett. **111,** 041301 (2013).

[15] P. A. R. Ade et al. (Planck Collaboration), Astron. Astrophys. **571,** A15 (2014).
[16] A. Moss, E. Copeland, S. Bamford, and T. Clarke, arXiv:2109.14848.
[17] A. G. Riess et al., Astrophys. J. Lett. **934,** L7 (2022).
[18] W. Hu and M. White, Astrophys. J. **471,** 30 (1996).
[19] M. Kopp, C. Skordis, and D. B. Thomas, Phys. Rev. D **94,** 043512 (2016).
[20] C.-P. Ma and E. Bertschinger, Astrophys. J. **455,** 7 (1995).
[21] K. A. Malik and D. Wands, Phys. Rep. **475,** 1 (2009).
[22] R. Durrer, Lect. Notes Phys. **653,** 31 (2004).
[23] R. H. Brandenberger, Lect. Notes Phys. **646,** 127 (2004).
[24] D. Baumann, *Cosmology* (Cambridge University Press, Cambridge, England, 2022).
[25] A. Riotto, *Lecture Notes on Cosmology* (CreateSpace Independent Publishing Platform, Scotts Valley, California, 2014).
[26] D. Blas, J. Lesgourgues, and T. Tram, J. Cosmol. Astropart. Phys. 07 (2011) 034.
[27] I. J. Allali, F. Rompineve, and M. P. Hertzberg, Phys. Rev. D **108,** 023527 (2023).
[28] N. Aghanim et al. (Planck Collaboration), Astron. Astrophys. **641,** A6 (2020).
[29] J. Torrado and A. Lewis, J. Cosmol. Astropart. Phys. 05 (2021) 057.

[30] W. J. Handley, M. P. Hobson, and A. N. Lasenby, Mon. Not. R. Astron. Soc. **450,** L61 (2015).

[31] N. Aghanim *et al.* (Planck Collaboration), Astron. Astrophys. **641,** A6 (2020).

[32] N. Aghanim *et al.* (Planck Collaboration), Astron. Astrophys. **641,** A8 (2020).

[33] E.-M. Mueller, W. Percival, E. Linder, S. Alam, G.-B. Zhao, A. G. Sánchez, F. Beutler, and J. Brinkmann, Mon. Not. R. Astron. Soc. **475,** 2122 (2018).

[34] F. Beutler, C. Blake, M. Colless, D. H. Jones, L. Staveley-Smith, L. Campbell, Q. Parker, W. Saunders, and F. Watson, Mon. Not. R. Astron. Soc. **416,** 3017 (2011).

[35] A. J. Ross, L. Samushia, C. Howlett, W. J. Percival, A. Burden, and M. Manera, Mon. Not. R. Astron. Soc. **449,** 835 (2015).

[36] D. M. Scolnic *et al.* (Pan-STARRS1 Collaboration), Astrophys. J. **859,** 101 (2018).

[37] C. Cartis, J. Fiala, B. Marteau, and L. Roberts. arXiv:1804.00154.

[38] C. Cartis, L. Roberts, and O. Sheridan-Methven, Optimization **71,** 2343 (2022).

[39] J. A. Nelder and R. Mead, Comput. J. (UK) **7,** 308 (1965).

[40] L. Herold, E. G. M. Ferreira, and E. Komatsu, Astrophys. J. Lett. **929,** L16 (2022).

[41] M. Raveri and W. Hu, Phys. Rev. D **99,** 043506 (2019).

[42] J. A. Sobrin *et al.* (SPT-3G Collaboration), Astrophys. J. Suppl. Ser. **258,** 42 (2022).

[43] T. M. C. Abbott *et al.* (DES Collaboration), Phys. Rev. D **105,** 023520 (2022).

[44] G. Ballesteros and J. Lesgourgues, J. Cosmol. Astropart. Phys. 10 (2010) 014.